ADVANCES IN ATMOSPHERIC SCIENCES, VOL. 38, SEPTEMBER 2021, 1596–1607

• **Original Paper** •

Re-examining Tropical Cyclone Fullness Using Aircraft Reconnaissance Data

Zhehan CHEN[†1] and Qingqing LI[*2,3]

[1]*Nanjing University of Information Science and Technology*, *Nanjing* 210044, *China*

[2]*Key Laboratory of Meteorological Disaster of the Ministry of Education*, *Nanjing University of Information Science and Technology*, *Nanjing* 210044, *China*

[3]*State Key Laboratory of Severe Weather*, *Chinese Academy of Meteorological Sciences*, *Beijing* 100081, *China*

(Received 30 August 2020; revised 14 March 2021; accepted 18 March 2021)

ABSTRACT

We use FLIGHT+ aircraft reconnaissance data for tropical cyclones (TCs) in the North Atlantic and Eastern Pacific from 1997 to 2015 to re-examine TC fullness (TCF) characteristics at the flight level. The results show a strong positive correlation between the flight-level TCF and the intensity of TCs, with the flight-level TCF increasing much more rapidly than the near-surface TCF with increasing intensity of the TCs. The tangential wind in small-TCF hurricanes is statistically significantly stronger near the eye center than that in large-TCF hurricanes. Large-TCF hurricanes have a ring-like vorticity structure. No significant correlation is observed between the flight-level TCF and the comparative extent of the vorticity-skirt region occupied in the outer core skirt. The proportion of the rapid filamentation zone in the outer core skirt increases with increasing flight-level TCF. The differences in entropy between the radius of the maximum wind and the outer boundary of the outer core skirt also increase with increasing flight-level TCF.

Key words: tropical cyclone, fullness, intensity, structure, aircraft reconnaissance data

Citation: Chen, Z. H., and Q. Q. Li, 2021: Re-examining tropical cyclone fullness using aircraft reconnaissance data. *Adv. Atmos. Sci.*, **38**(9), 1596–1607, https://doi.org/10.1007/s00376-021-0282-0.

Article Highlights:

- Flight-level fullness increases much more rapidly than the near-surface fullness with increasing tropical cyclone intensity.
- There is no correlation between the flight-level fullness and the extent of the vorticity skirt occupied in the outer core skirt.
- The proportion of the rapid filamentation zone in the outer core skirt increases with increasing flight-level fullness.

1. Introduction

Tropical cyclones (TCs) are devastating weather systems that can cause serious threats to both human life and property. The size of a TC is important in estimating its destructivity (Powell and Reinhold, 2007) and several different metrics can be used to measure this (Carrasco et al., 2014), such as the radius of the maximum wind (RMW), the outer radius of the vanishing wind, the radius of the outermost closed isobar, and the radius of certain wind velocity. Many studies have addressed the relationship between the size and intensity of TCs and the change in intensity, but the results vary. Merrill (1984) reported a weak correlation between the size of a TC, defined by the radius of the outermost closed isobar, and intensity, whereas Carrasco et al. (2014) found no relationship between the radius of the outermost closed isobar and changes in the intensity of North Atlantic hurricanes. Kimball and Mulekar (2004) showed that the RMW to be negatively correlated with the intensity of TCs, whereas a radius of 17 m s^{-1} (R_{17}) was positively correlated with intensity. By contrast, Wu et al. (2015) showed a nonlinear relationship between R_{17} and the intensity of TCs, indicating that R_{17} increases with the maximum wind speed of TCs increasing up to 53 m s^{-1} and then decreases as the intensity of TCs continues to increase. Song et al. (2020) reported that the nonlinear TC size–intensity relationship is only seen in recurving typhoons in the western North Pacific that have a peak in intensity and size at different

* Corresponding author: Qingqing LI
Email: liqq@nuist.edu.cn
† Current affiliation: Nanjing University

times. However, Carrasco et al. (2014) suggested that the RMW and R_{17} have the most significant negative correlation with hurricane intensity changes by analyzing the second-generation North Atlantic hurricane database and the Extended Best-Track dataset. More recently, Ma (2020) and Ma et al. (2020) further indicated that a cold-core oceanic eddy could decrease the radius of hurricane-force wind and increase the RMW while the TC tracked over the eddy region and weakened.

These results suggest that the exact relationship between the size of a TC measured by different metrics and the intensity remains unclear. Guo and Tan (2017) introduced a new concept to quantitatively interpret the wind structure of TCs, which they referred to as TC fullness (TCF). TCF is defined as the ratio of the radial extent between the near-surface RMW and R_{17} (namely the width of the outer core wind skirt) to R_{17}. Guo and Tan (2017) found that the intensity of TCs is more strongly correlated with TCF than other measures of size. They further suggested that, along with rapid growth in the TCF, a strong low-level inflow and the radially inward advection of the absolute angular momentum favor the intensification of TCs. A significant finding in Guo and Tan (2017) is that either small or large TCs can be intense, depending on the TCF. Note that although TCF was proposed to supplement TC size metrics, this concept is not explicitly related to a specific TC size measurement. As found in Guo and Tan (2017), a given TCF value can be associated with either small or large TCs measured with typical TC size metrics.

Guo and Tan (2017) used the Extended Best-Track dataset (Demuth et al., 2004, 2006) to calculate the TCF. The wind radii in this dataset are mainly estimated using parameters derived from the Advanced Microwave Sounding Unit instrument onboard National Oceanic and Atmospheric Administration (NOAA) and European satellites. The main drawback of using microwave data to estimate the size of a TC is that the microwave instrumentation is onboard polar-orbiting satellites and is therefore not available at synoptic times. In addition, the winds estimated using microwave remote sensing may have more significant uncertainties than scatterometry, which gives the most direct estimation of surface winds (Dean et al., 2009). It is unclear whether the TCF characteristics reported by Guo and Tan (2017) are different from those determined using in situ observations. We thus re-examine the characteristics of TCF based on the Extended Flight Level Dataset for TCs (FLIGHT+; Vigh et al., 2018), which includes in situ, flight-level observations from aircraft reconnaissance flights. Moreover, the relationships between the kinematic and thermodynamic characteristics of TCs and the TCF will be discussed as well.

The remainder of this paper is organized as follows. Section 2 introduces the data and methods. Sections 3 describes the characteristics of the flight-level TCF measured in the FLIGHT+ dataset. The relationships between the kinematic and thermodynamic characteristics of TCs and the TCF are presented in section 4. A summary is given in section 5.

2. Data and methods

2.1. *FLIGHT+ aircraft reconnaissance data*

The FLIGHT+ dataset includes 229 flight missions for 74 hurricanes from 1997 to 2015. FLIGHT+ consolidates in situ, flight-level data observed by the NOAA WP-3D (Aberson et al., 2006b) and US Air Force WC-130 aircraft. Figure 1a shows a flight path into Hurricane Rita by WP-3D aircraft on 21 September 2005, which is in the FLIGHT+ dataset and includes several radial flight legs during the penetration of the aircraft into the inner core of the hurricane. The FLIGHT+ dataset consists of observations from the radial flight legs. The radial legs where the radial extent is > 45 km and the aircraft flew within 25 km of the center of the TC (Fig. 1b) are defined as "good" radial legs. We only use the observations in "good" radial legs in this study. More information on the FLIGHT+ dataset is given in Martinez et al. (2017) and Vigh et al. (2018).

Aircraft reconnaissance missions into hurricanes are typically conducted at either 850 or 700 hPa, with the 850-hPa flight level mostly used for weak depressions and tropical storms. We only use the observations at 700 hPa in this study. During the passage through the TCs, water droplets may adhere to the sensors mounted on the aircraft exterior, which regularly generates instrument wetting errors (Eastin et al., 2002). In addition, the observed temperature may be underestimated as a result of evaporative cooling on the thermistors. The correction method introduced by Zipser et al. (1981) is adopted to remove these errors. Eastin et al. (2002) concluded that this correction method could reduce the average errors in temperature, specific humidity, and equivalent potential temperature to 0.6°C, 0.5 g kg^{-1}, and 2.7 K, respectively. About 9.7% of the observational samples used in this study are corrected (not shown), a relatively low proportion.

Because we will examine the azimuthal mean distributions of the kinematic and thermodynamic fields, we also need to ensure that the selected "good" radial legs are relatively evenly distributed in the main quadrants (Fig. 1b). Therefore, the azimuthal mean values of a hurricane for each flight mission are calculated by averaging all of the "good" radial legs at each radial point. Figure 1c shows the azimuthal mean structures of the temperature and tangential wind in a flight mission into Hurricane Rita (2005) on 21 September 2005. The maximum tangential wind and the RMW at the flight level at that time were about 65 m s^{-1} and 25 km, respectively, with an apparent warm-core structure and a temperature maximum of 28°C within the eye.

2.2. *Intensity of TCs*

We do not use the FLIGHT+ wind velocity to estimate the intensity of TCs in this study because the flight-level velocity is not routinely used to measure the intensity of TCs and the observations for the flight legs are insufficient to capture the maximum wind speed within the circulation of a TC. We use the intensity of TCs derived from the National

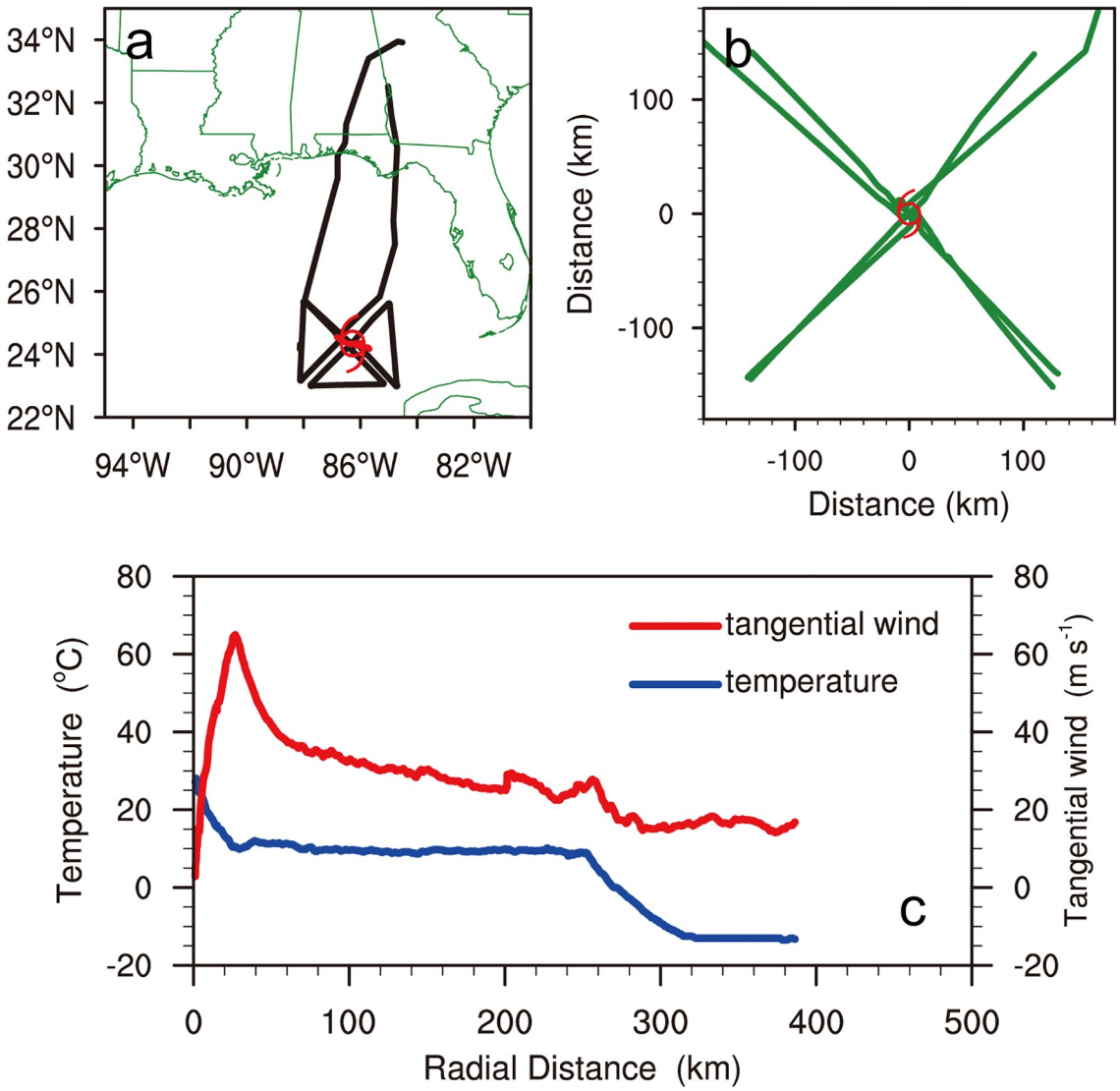

Fig. 1. (a) Flight path (black line) through Hurricane Rita on 21 September 2005. The red hurricane symbol denotes the center of the hurricane determined using the method proposed by Willoughby and Chelmow (1982). (b) Example of "good" radial legs (green lines) relative to the center of the TC. (c) Azimuthal mean profiles of the tangential wind (red line; m s^{-1}) and temperature (blue line; °C) of "good" radial legs in a flight mission into Hurricane Rita on 21 September 2005.

Hurricane Center Best-Track dataset. The best-track data are available at standard synoptic times (0000, 0600, 1200, and 1800 UTC), but the average flight mission times are generally mismatched with the standard synoptic times. To obtain the intensity of TCs at the FLIGHT+ record times, we linearly interpolate the maximum sea-level wind velocity (V_{max}) and the minimum sea-level pressure (P_{min}) from the best-track data at two adjacent standard synoptic times to the corresponding average flight mission time. The interpolated intensity of the TC can be used to reasonably represent the intensity of a TC at the average flight mission time because the change in intensity between two adjacent standard synoptic times is generally not large.

2.3. *TCF calculation*

Guo and Tan (2017) defined TCF as the ratio of the radial extent between the RMW and R_{17} to R_{17} at the surface. We focus on the TCF at 700 hPa based on the FLIGHT+ dataset. Previous studies have suggested that the wind speed of TCs at sea level is about 85% of the wind speed at the 700-hPa flight level (Shea and Gray, 1973; Powell, 1982; Jorgensen, 1984a; Powell et al., 2009). Here, the radius of the 20 m s^{-1} wind speed is applied to represent the outer boundary of the outer core wind skirt of TCs. The TCF at the flight level is thus formulated as:

$$\mathrm{TCF} = \frac{R_{20} - \mathrm{RMW}_{700\,\mathrm{hPa}}}{R_{20}} = 1 - \frac{\mathrm{RMW}_{700\,\mathrm{hPa}}}{R_{20}}, \qquad (1)$$

where $\mathrm{RMW}_{700\ \mathrm{hPa}}$ is the mean RMW at 700 hPa in the "good" radial flight legs. Similarly, R_{20} is the azimuthal mean of the 20 m s^{-1} wind speed radius in the "good" radial

legs. An 11-point smoothing method is used to remove fine-scale features in the wind field outside the RMW when we estimate R_{20}. The box-and-whisker plot in Fig. 2 shows that the bottom and top quartiles of $RMW_{700\ hPa}$ are 18 and 75 km, respectively, whereas the bottom and top quartiles of R_{20} are 100 and 197 km, respectively. TCs at different stages show distinct values of $RMW_{700\ hPa}$ and R_{20} (not shown).

Following Guo and Tan (2017), we classify the flight-level TCF into four categories: FS1 (TCF ⩽ 0.4); FS2 (0.4 < TCF ⩽ 0.6); FS3 (0.6 < TCF ⩽ 0.8); and FS4 (TCF > 0.8). The numbers of the flight missions satisfying the four TCF categories are 28, 50, 94, and 57, respectively.

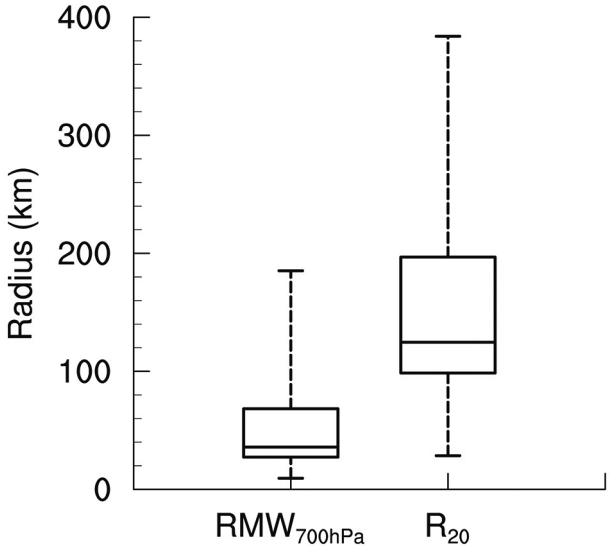

Fig. 2. Box-and-whisker plots of $RMW_{700\ hPa}$ and R_{20} calculated using the FLIGHT+ aircraft reconnaissance dataset. The interior line indicates the median, the boxes extend to the 25th and 75th percentiles, and the whiskers extend to the minimum and maximum values.

3. Characteristics of the flight-level TCF

Figure 3 shows the relationship of TCF with V_{max}, $RMW_{700\ hPa}$, and R_{20}. For most category 3 and more intense hurricanes (V_{max} > 50 m s^{-1}), the radii of the maximum wind speed are < 60 km and the radii of the 20 m s^{-1} wind speed are > 100 km. Not surprisingly, $RMW_{700\ hPa}$ tends to decrease with increasing V_{max}, with a correlation coefficient of −0.4204 at the 95% confidence level. By contrast, the correlation coefficient between TCF and V_{max} reaches 0.7088 and that between TCF and P_{min} is −0.6468 at the 95% confidence level. Specifically, the TCF values of the majority of intense TCs (V_{max} > 50 m s^{-1}) are > 0.6 (Fig. 3). Therefore, similar to the near-surface TCF results in Guo and Tan (2017), a larger flight-level TCF corresponds to a more intense hurricane. In addition, there is virtually no correlation between TCF and both R_{20} and $RMW_{700\ hPa}$ (Fig. 3), consistent with the result in Guo and Tan (2017).

The scatter diagrams in Fig. 4 indicate that there is a nonlinear relationship between TCF and the intensity of a TC. We use a curve-fitting method to fit the relationship between TCF and the intensity of a TC. Power functions are found to express the relationship between TCF and V_{max} and P_{min} reasonably well. The red curve in Fig. 4a shows the best-fit result for the relationship between the flight-level TCF and V_{max}, which is given by:

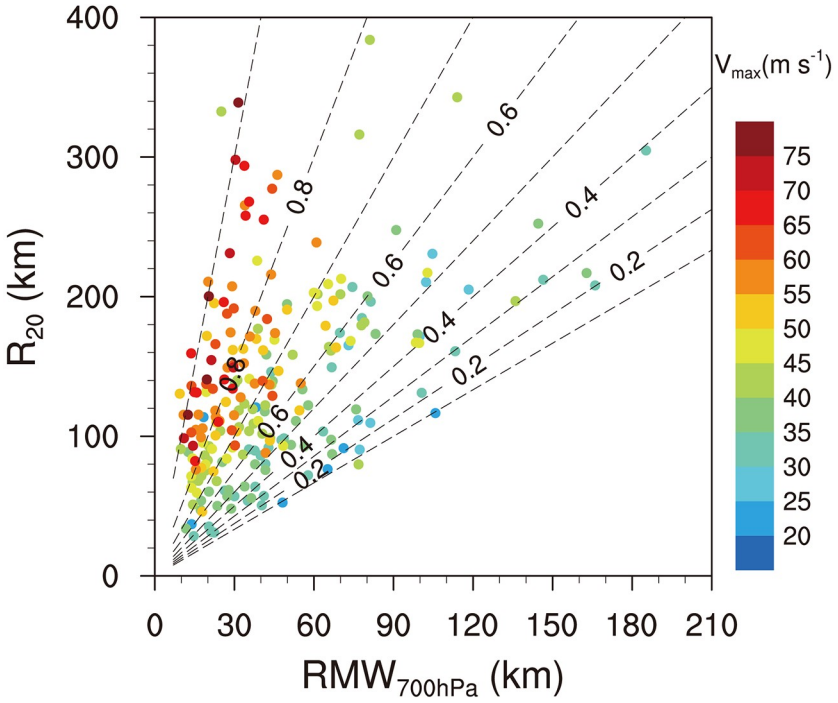

Fig. 3. Dependence of V_{max} (colored dots; m s^{-1}) on $RMW_{700\ hPa}$ (km), R_{20} (km), and the TCF (dashed lines).

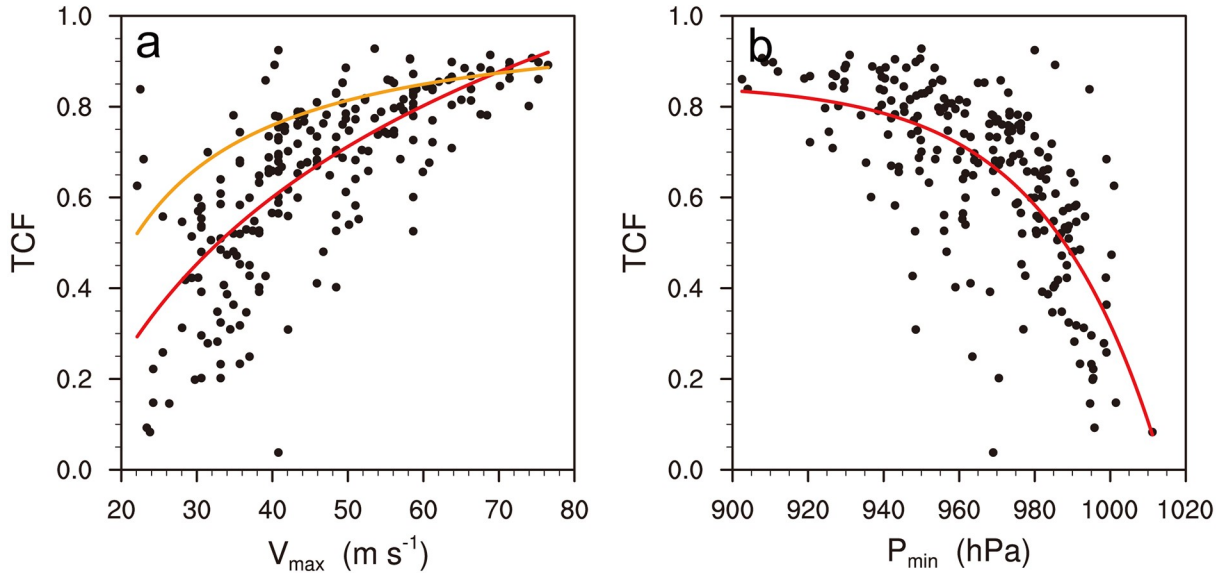

Fig. 4. (a) Scatter diagram of V_{max} (m s^{-1}) versus the TCF. The red curve shows the best-fit result for the relationship between the flight-level TCF and V_{max} and the orange curve shows the best-fit result of Guo and Tan (2017). (b) Scatter diagram of P_{min} (hPa) and the TCF. The red curve shows the best-fit result.

$$\mathrm{TCF} = 6.92 - 6.68 \times \left(\frac{V_{max}}{V_{20}}\right)^{-0.08}, \qquad (2)$$

where $V_{20} = 20$ m s^{-1}. The coefficient of determination for the best-fit curve in Fig. 4a is 0.52 at the 95% confidence level. The best-fit curve (orange curve) representing the relationship between the near-surface TCF and V_{max} in Guo and Tan (2017) is also plotted in Fig. 4a. Those two curves behave differently, although both show TCF increasing with the intensity of the TC (Fig. 4a). In particular, the flight-level TCF increases much more rapidly with increasing V_{max} than the near-surface TCF. Regardless of the differences in the data used here and in Guo and Tan (2017), the outer boundary of the outer core wind skirt seems to expand more slowly near the surface than at the flight level during the intensification of a TC, possibly as a result of acceleration abated by surface friction.

Figure 4b shows the relationship between the flight-level TCF and P_{min}, which also suggests that TCF increases with increasing intensity of a TC. The relationship can be fitted with a power function as follows:

$$\mathrm{TCF} = 0.85 - 0.53 \times \left(\frac{P_{min}}{P_0}\right)^{33.99}, \qquad (3)$$

where $P_0 = 1000$ hPa.

4. Kinematic and thermodynamic characteristics of TCs associated with the flight-level TCF

4.1. *Kinematic characteristics*

Figure 5a shows the relationships between the flight-level TCF and the difference in the tangential wind velocity at $\mathrm{RMW}_{700\ \mathrm{hPa}}$ and R_{20}. Figure 5a shows that the higher the TCF, the higher the difference in the tangential wind velocity. In particular, when TCF > 0.6, the difference in the tangential wind velocity at $\mathrm{RMW}_{700\ \mathrm{hPa}}$ and R_{20} increases more rapidly with the TCF. As noted above, the TCF is related to the TC intensity. Figure 5a indicates that the difference in the tangential wind velocity at $\mathrm{RMW}_{700\ \mathrm{hPa}}$ and R_{20} is also related to the hurricane intensity, with a full correlation coefficient of 0.83 at the 95% confidence level. Therefore, it is difficult to attribute the TCF exclusively to the difference in the tangential wind velocity. Here we utilize partial correlations to isolate the TCF response to the difference in the tangential wind velocity after controlling for changes in the TC intensity and the tangential wind velocity difference. Similar partial correlations are evaluated to examine the relationships between the TCF and other variables. The partial correlation coefficient between the TCF and the difference in the tangential wind velocity is 0.61 at the 95% confidence level. This result indicates that the difference in the tangential wind velocity at $\mathrm{RMW}_{700\ \mathrm{hPa}}$ and R_{20} indeed increases with increasing TCF.

Figure 5b shows the composites of the flight-level tangential wind velocity normalized by the tangential wind at R_{20} for different categories of TCF. Note that the radius is also normalized by $\mathrm{RMW}_{700\ \mathrm{hPa}}$. The normalized tangential wind of FS1 hurricanes is statistically significantly stronger than that of FS2, FS3, and FS4 hurricanes within a distance of one-half the $\mathrm{RMW}_{700\ \mathrm{hPa}}$ from the storm center. This possibly reflects the presence of hub convection rather than a visible eye near the center of the relatively weak TCs with a small TCF. The tangential wind at $\mathrm{RMW}_{700\ \mathrm{hPa}}$ increases markedly with an increase in TCF, consistent with the relationship between the TC intensity and the TCF.

Figure 6a shows the relationship between the flight-level TCF and the relative vorticity difference at $RMW_{700\ hPa}$ and R_{20}. As expected, the relative vorticity difference tends to increase with increasing TCF, with a partial correlation coefficient of 0.5 at the 95% confidence level. Figure 6b shows the relative vorticity composites for different categories of TCF normalized by the vorticity at R_{20}. The FS4 hurricanes have much higher vorticity near the RMW than other categories. FS3 and FS4 hurricanes clearly show a ring-like vorticity structure, coincident with the greater intensity of these hurricanes. Schubert et al. (1999) showed that such an annular structure of vorticity favors exponential barotropic instability. By contrast, the annular vorticity structure is not apparent in FS1 and FS2 hurricanes (Fig. 6b).

The difference in absolute angular momentum between $RMW_{700\ hPa}$ and R_{20} is negatively correlated with the TCF (Fig. 7a) with a weak partial correlation coefficient of −0.2 at the 95% confidence level. The composites of the absolute angular momentum normalized by the absolute angular momentum at R_{20} show that the absolute angular momentum increases with the radius (Fig. 7b), in agreement with the results of previous studies. The normalized absolute angular momentum is largest for FS1 hurricanes, particularly near the RMW, and smallest for FS4 hurricanes, with FS2 and FS3 hurricanes in between. Compared to hurricanes with larger TCF, hurricanes with smaller TCF generally show larger absolute angular momentum at the RMW because the RMW is larger (Fig. 3), while absolute angular

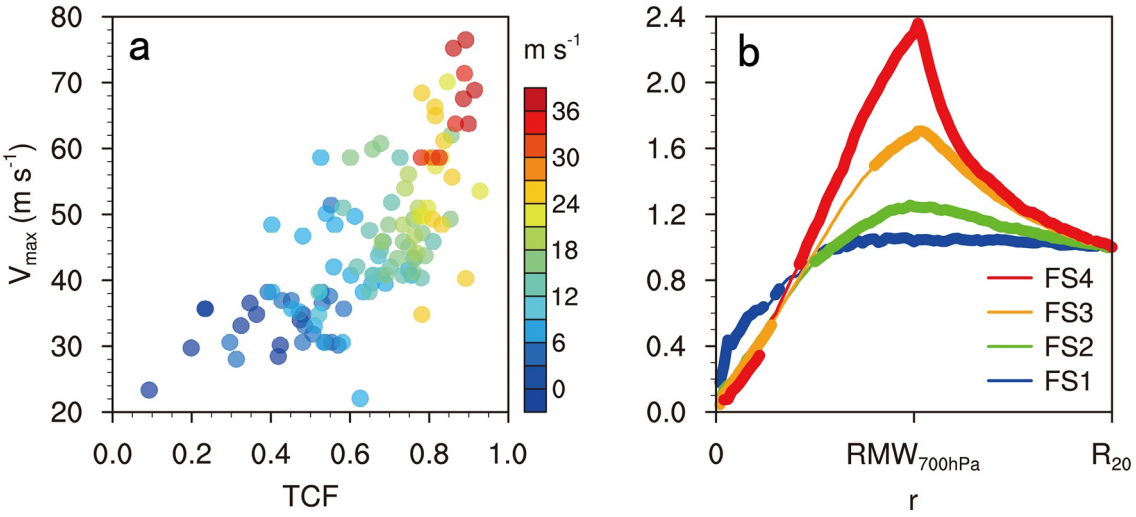

Fig. 5. (a) Dependence of the difference in the flight-level tangential wind (m s^{-1}) at $RMW_{700\ hPa}$ and R_{20} on the TCF and V_{max}. (b) Composites of the normalized flight-level tangential wind corresponding to different categories of TCF. The bold lines indicate that the composite results are statistically significant at the 95% confidence level and the radius is normalized by the $RMW_{700\ hPa}$.

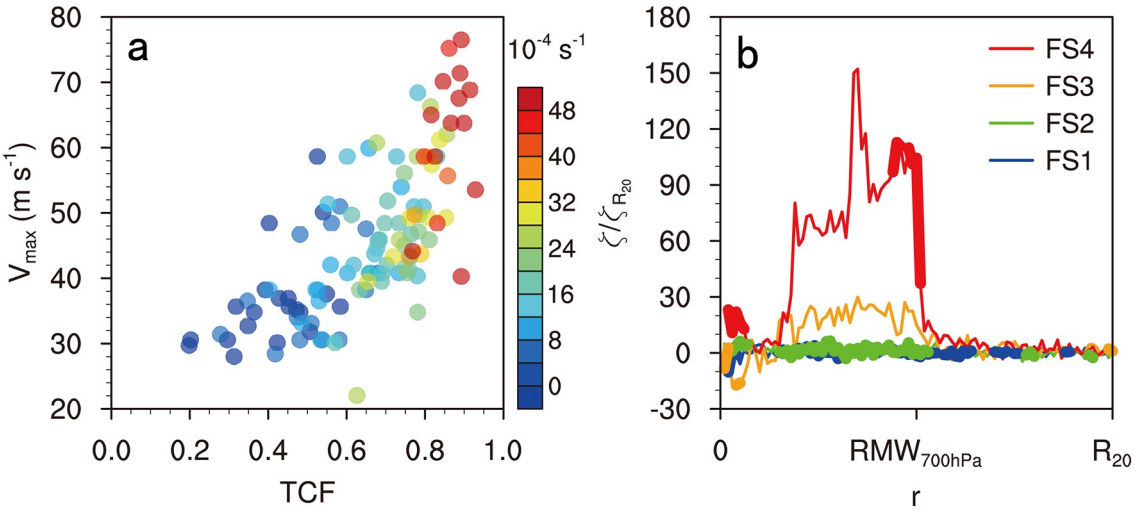

Fig. 6. (a) Dependence of the difference in the flight-level vertical vorticity (10^{-4} s^{-1}) at $RMW_{700\ hPa}$ and R_{20} on the TCF and V_{max}. (b) Composites of the normalized flight-level vertical vorticity corresponding to different categories of TCF. The bold lines indicate that the composite results are statistically significant at the 95% confidence level and the radius is normalized by the $RMW_{700\ hPa}$.

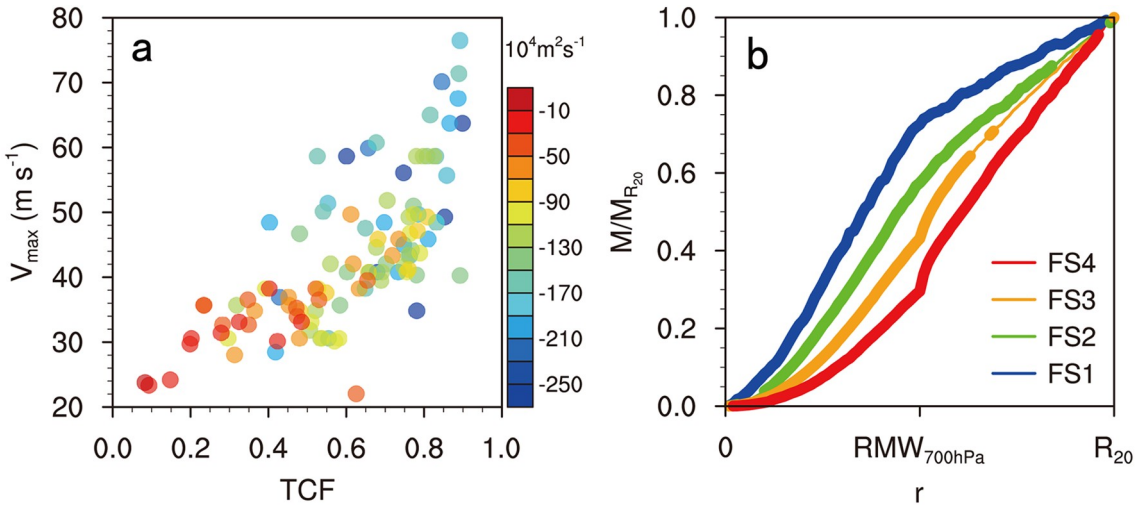

Fig. 7. (a) Dependence of the difference in the flight-level absolute angular momentum (10^4 m^2 s^{-1}) at RMW$_{700\ hPa}$ and R_{20} on the TCF and V_{max}. (b) Composites of the normalized flight-level absolute angular momentum corresponding to different categories of TCF. The bold lines indicate that the composite results are statistically significant at the 95% confidence level and the radius is normalized by the RMW$_{700\ hPa}$.

momentum is smaller at R_{20} because R_{20} is smaller (Fig. 3). As a result, FS1 hurricanes exhibit the largest normalized absolute angular momentum near the RMW.

Radial gradients in the potential vorticity play an essential part in the formation of vortex Rossby waves (Montgomery and Kallenbach, 1997). The activity of vortex Rossby waves has striking effects on the intensity of TCs and changes in their structure (Wang, 2002a, b; Li and Wang, 2012a; Li et al., 2014, 2017). The radial extent of the potential vorticity skirt determines the area in which vortex Rossby waves are active. Because the TCF depends on the outer core skirt, an interesting question is whether there is a relationship between the TCF and the region in which vortex Rossby waves form and propagate radially outward. Shapiro and Montgomery (1993) defined an effective beta value $[-(\partial\bar{q}\bar{\xi})/(\partial r\bar{q})$, where $\bar{\xi} = f + 2\bar{V}/r$ is the inertial parameter, V is the tangential wind, q is the potential vorticity, r is the radius, and the overbar denotes the azimuthal mean] to describe the potential vorticity skirt. The region in which the effective beta value is positive favors the formation and development of vortex Rossby waves. Because it is difficult to calculate the potential vorticity based on the FLIGHT+ data, we define a quasi-effective beta (β_{qua}) as follows:

$$\beta_{qua} = -\frac{\partial\bar{\zeta}}{\partial r}\frac{\bar{\xi}}{\bar{\zeta}}, \tag{4}$$

where $\bar{\zeta}$ represents the azimuthal mean relative vorticity. Figure 8a shows that there is no significant correlation between the TCF and the proportion of the region with a positive quasi-effective beta in the region between RMW$_{700\ hPa}$ and R_{20}. The comparative extent of the (potential) vorticity-skirt region in the outer core skirt, where vortex Rossby waves tend to form and develop, is not related to the TCF at the flight level.

There is a pronounced deformative region immediately outside the eyewall in the inner core (Rozoff et al., 2006; Wang, 2008; Li and Wang, 2012b). Rozoff et al. (2006) defined the filamentation time (τ_{fil}) to evaluate this horizontal deformation effect:

$$\tau_{fil} = \left(-\frac{\bar{V}}{r}\frac{\partial\bar{V}}{\partial r}\right)^{\frac{1}{2}}. \tag{5}$$

Rozoff et al. (2006) showed that strong horizontal deformation inhibits deep cellular convection formation, thus forming the moat in the inner core of TCs. The region with $\tau_{fil} \leqslant 45$ min is defined as the rapid filamentation zone, which favors the development of organized inner spiral rainbands (Wang, 2008; Li and Wang, 2012b).

Figure 8b suggests that the proportion of the rapid filamentation zone in the region between RMW$_{700\ hPa}$ and R_{20} tends to increase with an increase in the TCF with a partial correlation coefficient of 0.3 at the 95% confidence level. This result shows that active inner rainbands may be observed in more extensive regions within the outer core skirt, of TCs with a greater TCF (Wang, 2008; Li and Wang, 2012b), assuming that the variation in RMW is comparatively small.

A radius of three or four times the RMW is roughly defined in many studies as the outer boundary of the inner core (Wang, 2008; Li and Wang, 2012a, b; Li et al., 2017), within which inner rainbands are usually observed. However, our result indicates that the relative extent of the rapid filamentation zone varies with the TCF. Therefore defining a fixed radius as the outer boundary of the inner core of a TC with a varying TCF remains arguable. In addition, we suggest that when the RMW is decreasing and the TCF is increasing in intensifying TCs, the rapid filamentation zone

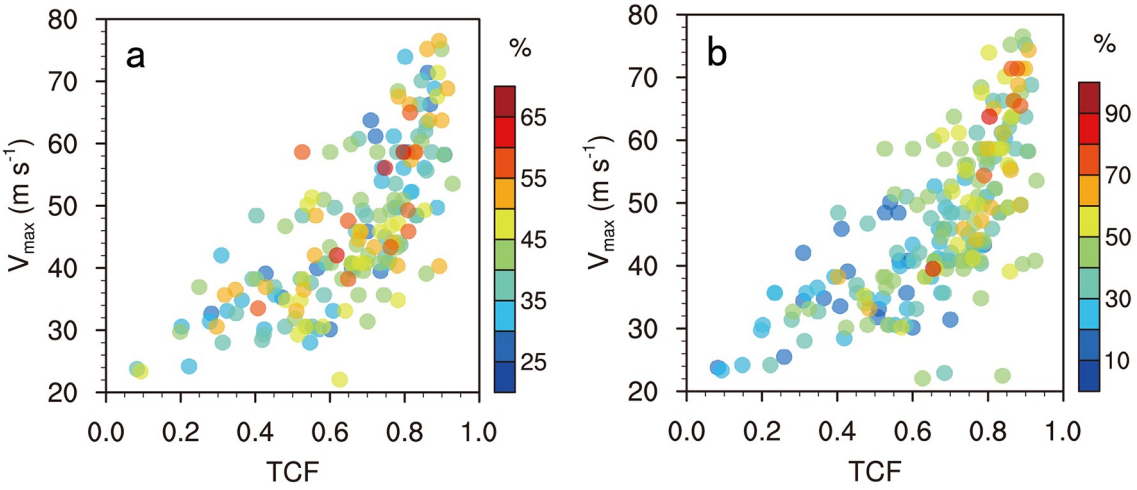

Fig. 8. Dependence of the proportions of (a) the region of positive quasi-effective beta and (b) the rapid filamentation zone in the region between $RMW_{700\ hPa}$ and R_{20} on the TCF and V_{max}.

tends to broaden. This broadening of the rapid filamentation zone means that more inner rainbands will develop in this region, and more diabatic heating induced by the inner rainbands will be produced. This scenario can contribute to further intensification of the TC (Li et al., 2014), which might be one of the reasons why more intense TCs tend to have a larger TCF (Figs. 3 and 4).

4.2. *Thermodynamic characteristics*

Figure 9a shows that the temperature differences between $RMW_{700\ hPa}$ and R_{20} are statistically significantly correlated with the TCF with a partial correlation coefficient of up to 0.53 at the 95% confidence level. The increase in the difference in temperature with increasing TCF again indicates that more active eyewall convection in more intense TCs with a larger TCF tends to produce stronger diabatic heating. This is also seen in Fig. 9b, which shows higher normalized temperatures near RMW for FS3 and FS4 hurricanes. Figure 9b shows temperature maxima near the center of the TC for FS1, FS2, and FS3 hurricanes, indicating the existence of a warm-core structure. TCs with a larger TCF have a more significant warm core. However, the composite temperature maximum of FS4 hurricanes occurs just inward of the RMW rather than near the center of the TC (Fig. 9b), with the inner core temperature characterized by a warm-ring structure. This feature seems to be consistent with the results of Schubert et al. (2007). They documented that remarkable subsidence tends to occur immediately on the inner side of the eyewall of intense TCs rather than at the center of the eye as a result of the large inertial stability, resulting in significant adiabatic heating.

The humidity differences between $RMW_{700\ hPa}$ and R_{20} also tend to increase with increasing TCF (Fig. 10a). The normalized humidity is at a maximum near the RMW for FS4

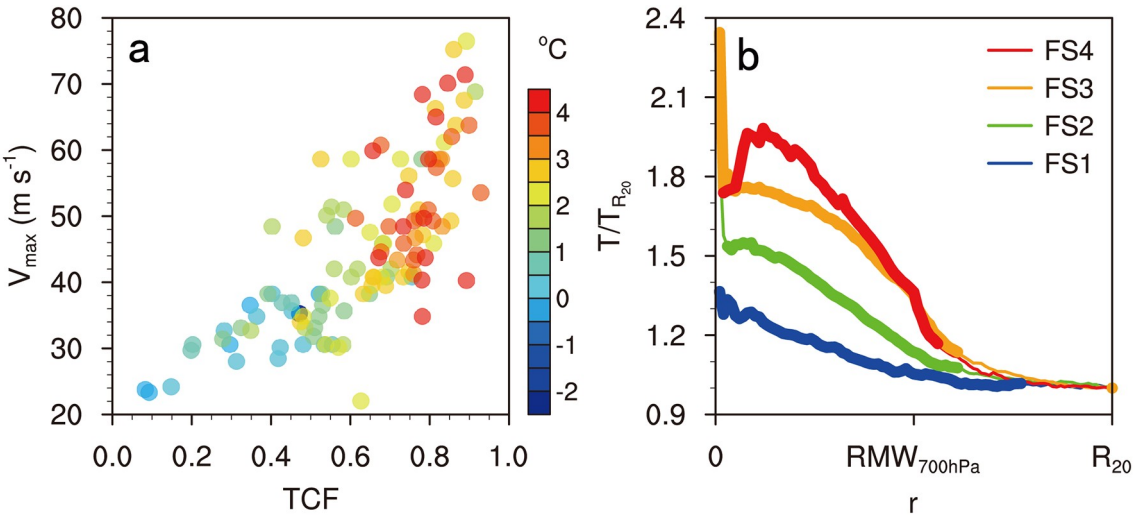

Fig. 9. (a) Dependence of the difference in the flight-level temperature (°C) at $RMW_{700\ hPa}$ and R_{20} on the TCF and V_{max}. (b) Composites of the normalized flight-level temperature corresponding to different categories of TCF. The bold lines indicate that the composite results are statistically significant at the 95% confidence level and the radius is normalized by the $RMW_{700\ hPa}$.

hurricanes, whereas it peaks at the center of the eye for FS1 and FS2 hurricanes (Fig. 10b). The maximum humidity near the RMW for FS4 hurricanes arises from the active eyewall convection that vertically advects moisture from the surface. The maximum low-level humidity at the center of the eye for FS1 and FS2 hurricanes is probably related to the existence of hub clouds in the eye (Simpson, 1952, 1955; Jordan, 1961; Willoughby, 1998; Aberson et al., 2006a).

Figure 11a shows that the differences in the equivalent potential temperature (θ_e) between $RMW_{700\ hPa}$ and R_{20} tend to increase with increasing TCF. The partial correlation coefficient between the TCF and the difference in θ_e is 0.43 at the 95% confidence level. Figure 11b shows the composite θ_e normalized by the θ_e value at R_{20}. An increased θ_e (an entropy excess) appears near the center of the eye, and similar phenomena have been found in other studies (Hawkins and Imbembo, 1976; Jorgensen, 1984b; Willoughby, 1998; Eastin et al., 2002; Schneider and Barnes, 2005; Montgomery et al., 2006; Sitkowski and Barnes, 2009). For FS4 hurricanes, the maximum θ_e is near the eyewall (Fig. 11b), matching the expectation of both empirical (Malkus and Riehl, 1960) and theoretical arguments (Emanuel, 1986).

5. Concluding remarks

A new concept, TCF, was proposed by Guo and Tan (2017) to describe the relationship between the intensity and size of TCs. TCF was initially defined as the ratio of the

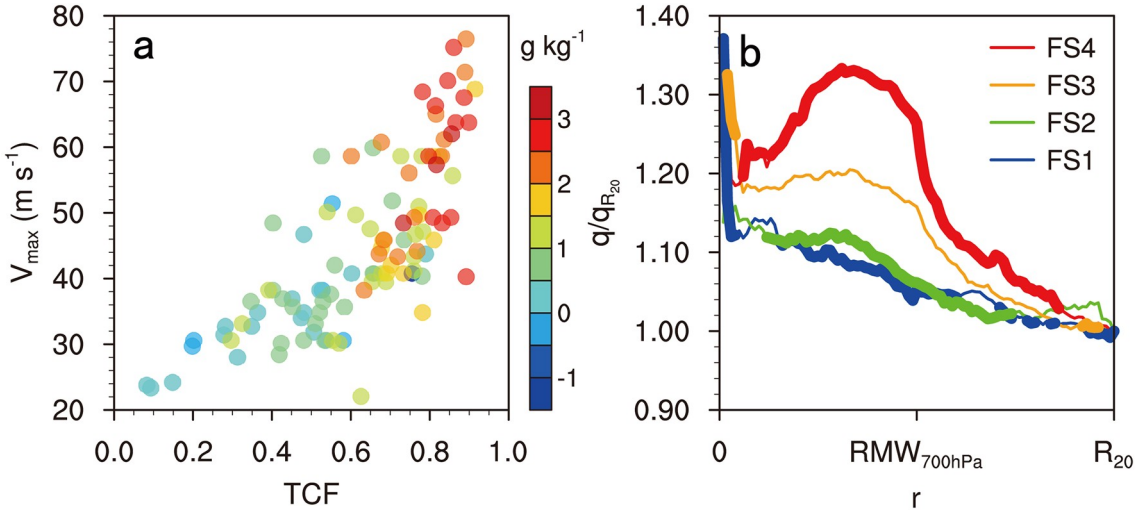

Fig. 10. (a) Dependence of the difference in the flight-level specific humidity (g kg^{-1}) at $RMW_{700\ hPa}$ and R_{20} on the TCF and V_{max}. (b) Composites of the normalized flight-level specific humidity corresponding to different categories of TCF. The bold lines indicate that the composite results are statistically significant at the 95% confidence level and the radius is normalized by the $RMW_{700\ hPa}$.

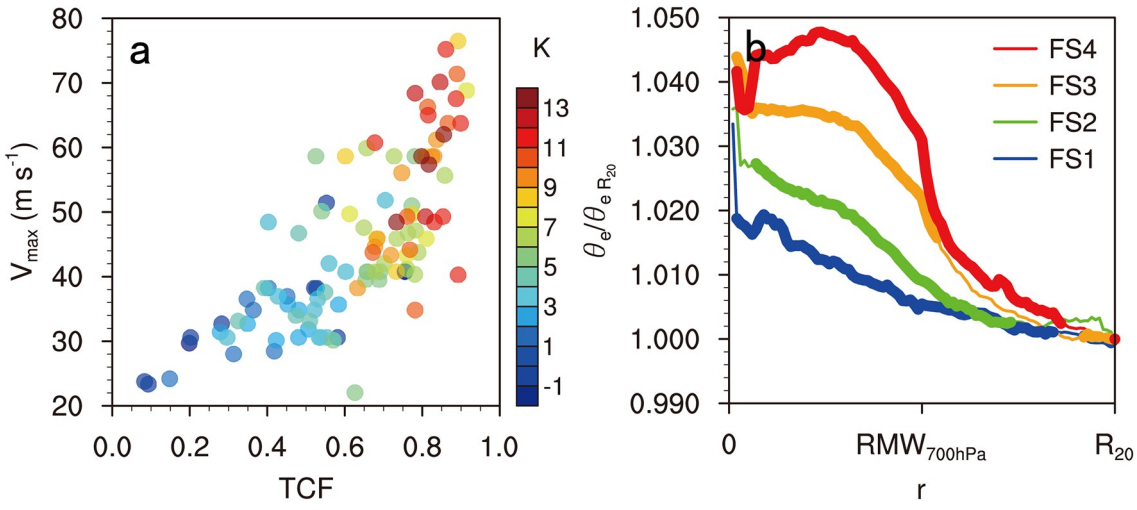

Fig. 11. (a) Dependence of the difference in the flight-level θ_e (K) at $RMW_{700\ hPa}$ and R_{20} on the TCF and V_{max}. (b) Composites of the normalized flight-level θ_e corresponding to different categories of TCF. The bold lines indicate that the composite results are statistically significant at the 95% confidence level and the radius is normalized by the $RMW_{700\ hPa}$.

radial extent between the near-surface RMW and R_{17} to R_{17}. Guo and Tan (2017) documented the characteristics of TCF based on the Extended Best-Track dataset in which the wind radii are estimated in terms of the data retrieved from satellites. The most insightful finding in Guo and Tan (2017) is that the intensity of TCs is more strongly correlated with TCF than with other measures of the size of a TC. To further examine whether the characteristics of TCF change when the TCF is evaluated with direct observations, we use in situ, flight-level observations from aircraft reconnaissance flights to calculate the flight-level TCF.

Similar to the results in Guo and Tan (2017), we found a strong positive correlation between the flight-level TCF and the intensity of TCs. In particular, the flight-level TCF of most TCs with $V_{max} > 50$ m s^{-1} exceeds 0.6. Compared to Guo and Tan (2017), however, the flight-level TCF tends to increase much more rapidly than the near-surface TCF with an increasing V_{max}.

The kinematic and thermodynamic features associated with the TCs with different flight-level TCF values were also investigated. FS3 and FS4 hurricanes have a ring-like vorticity structure. No significant correlation is found between the flight-level TCF and the comparative extent of the (potential) vorticity-skirt region occupied in the outer core skirt. The proportion of the rapid filamentation zone in the outer core skirt increases with increasing flight-level TCF, indicating that inner rainbands may develop in more extensive regions for TCs with a larger TCF. FS1, FS2, and FS3 hurricanes show a more significant inner warm core, whereas FS4 hurricanes are characterized by a warm-ring structure. The θ_e differences between $RMW_{700\ hPa}$ and R_{20} tend to increase with an increase in the flight-level TCF.

Based on in situ, flight-level observations from aircraft reconnaissance, we show that the TCF can be used to describe the relationship between the intensity of a TC and the entire structure of the wind field. There are several shortcomings regarding the flight-level TCF discussed here. For instance, the TCF calculation is based on observations from several radial flight legs, which may lead to observational undersampling of the TC wind fields. In addition, TCF cannot represent the azimuthally asymmetric wind field structures of TCs in complex environments.

Acknowledgements. We thank two anonymous reviewers for their reviews. We are greatly grateful to Dr. Jonathan L. VIGH for providing the Extended Flight Level Dataset (FLIGHT+) for tropical cyclones. The FLIGHT+ was created by the Research Applications Laboratory at the National Center for Atmospheric Research (NCAR) from data provided by the NOAA Hurricane Research Division of AOML and the U.S. Air Force Reserve. This work was jointly supported by the National Key Research and Development Program of China under Grant 2017YFC1501601, the Key Program of the Ministry of Science and Technology of China under Grant 2017YFE0107700, and the National Natural Science Foundation of China under Grants 41875054, 41730961, 41730960, and 41775065.

REFERENCES

Aberson, S. D., J. P. Dunion, and F. D. Marks, 2006a: A photograph of a wavenumber-2 asymmetry in the Eye of Hurricane Erin. *J. Atmos. Sci.*, **63**, 387–391, https://doi.org/10.1175/JAS3593.1.

Aberson, S. D., M. L. Black, R. A. Black, R. W. Burpee, J. J. Cione, C. W. Landsea, and F. D. Marks, 2006b: Thirty years of tropical cyclone research with the NOAA P-3 aircraft. *Bull. Amer. Meteor. Soc.*, **87**, 1039–1056, https://doi.org/10.1175/BAMS-87-8-1039.

Carrasco, C. A., C. W. Landsea, and Y.-L. Lin, 2014: The influence of tropical cyclone size on its intensification. *Wea. Forecasting*, **29**, 582–590, https://doi.org/10.1175/WAF-D-13-00092.1.

Dean, L., K. A. Emanuel, and D. R. Chavas, 2009: On the size distribution of Atlantic tropical cyclones. *Geophys. Res. Lett.*, **36**, L14803, https://doi.org/10.1029/2009GL039051.

Demuth, J. L., M. DeMaria, J. A. Knaff, and T. H. Vonder Haar, 2004: Evaluation of Advanced Microwave Sounding Unit tropical-cyclone intensity and size estimation algorithms. *J. Appl. Meteorol.*, **43**, 282–296, https://doi.org/10.1175/1520-0450(2004)043<0282:EOAMSU>2.0.CO;2.

Demuth, J. L., M. DeMaria, and J. A. Knaff, 2006: Improvement of advanced microwave sounding unit tropical cyclone intensity and size estimation algorithms. *J. Appl. Meteorol. Climatol.*, **45**, 1573–1581, https://doi.org/10.1175/JAM2429.1.

Eastin, M. D., P. G. Black, and W. M. Gray, 2002: Flight-level thermodynamic instrument wetting errors in Hurricanes. Part I: Observations. *Mon. Wea. Rev.*, **130**, 825–841, https://doi.org/10.1175/1520-0493(2002)130<0825:FLTIWE>2.0.CO;2.

Emanuel, K. A., 1986: An air-sea interaction theory for tropical cyclones. Part I: Steady-state maintenance. *J. Atmos. Sci.*, **43**, 585–604, https://doi.org/10.1175/1520-0469(1986)043<0585:AASITF>2.0.CO;2.

Guo, X., and Z.-M. Tan, 2017: Tropical cyclone fullness: A new concept for interpreting storm intensity. *Geophys. Res. Lett.*, **44**, 4324–4331, https://doi.org/10.1002/2017GL073680.

Hawkins, H. F., and S. M. Imbembo, 1976: The structure of a small, intense hurricane—Inez 1966. *Mon. Wea. Rev.*, **104**, 418–442, https://doi.org/10.1175/1520-0493(1976)104<0418:TSOASI>2.0.CO;2.

Jordan, C. L., 1961: Marked changes in the characteristics of the eye of intense typhoons between the deepening and filling stages. *J. Atmos. Sci.*, **18**, 779–789, https://doi.org/10.1175/1520-0469(1961)018<0779:MCITCO>2.0.CO;2.

Jorgensen, D. P., 1984a: Mesoscale and convective-scale characteristics of mature hurricanes. Part I: General observations by research aircraft. *J. Atmos. Sci.*, **41**, 1268–1285, https://doi.org/10.1175/1520-0469(1984)041<1268:MACSCO>2.0.CO;2.

Jorgensen, D. P., 1984b: Mesoscale and convective-scale characteristics of mature hurricanes. Part II. Inner core structure of Hurricane Allen (1980). *J. Atmos. Sci.*, **41**, 1287–1311, https://doi.org/10.1175/1520-0469(1984)041<1287:MACSCO>2.0.CO;2.

Kimball, S. K., and M. S. Mulekar, 2004: A 15-year climatology

of North Atlantic tropical cyclones. Part I: Size parameters. *J. Climate*, **17**, 3555–3575, https://doi.org/10.1175/1520-0442(2004)017<3555:AYCONA>2.0.CO;2.

Li, Q. Q., and Y. Q. Wang, 2012a: Formation and quasi-periodic behavior of outer spiral rainbands in a numerically simulated tropical cyclone. *J. Atmos. Sci.*, **69**, 997–1020, https://doi.org/10.1175/2011JAS3690.1.

Li, Q. Q., and Y. Q. Wang, 2012b: A comparison of inner and outer spiral rainbands in a numerically simulated tropical cyclone. *Mon. Wea. Rev.*, **140**, 2782–2805, https://doi.org/10.1175/MWR-D-11-00237.1.

Li, Q. Q., Y. Q. Wang, and Y. H. Duan, 2014: Effects of diabatic heating and cooling in the rapid filamentation zone on structure and intensity of a simulated tropical cyclone. *J. Atmos. Sci.*, **71**, 3144–3163, https://doi.org/10.1175/JAS-D-13-0312.1.

Li, Q. Q., Y. Q. Wang, and Y. H. Duan, 2017: A numerical study of outer rainband formation in a sheared tropical cyclone. *J. Atmos. Sci.*, **74**, 203–227, https://doi.org/10.1175/JAS-D-16-0123.1.

Ma, Z. H., 2020: A study of the interaction between Typhoon Francisco (2013) and a cold-core eddy. Part I: Rapid weakening. *J. Atmos. Sci.*, **77**, 355–377, https://doi.org/10.1175/JAS-D-18-0378.1.

Ma, Z. H., J. F. Fei, X. G. Huang, X. P. Cheng, and L. Liu, 2020: A study of the interaction between Typhoon Francisco (2013) and a cold-core eddy. Part II: Boundary layer structures. *J. Atmos. Sci.*, **77**, 2865–2883, https://doi.org/10.1175/JAS-D-19-0339.1.

Malkus, J. S., and H. Riehl, 1960: On the dynamics and energy transformations in steady-state hurricanes. *Tellus*, **12**, 1–20, https://doi.org/10.1111/j.2153-3490.1960.tb01279.x.

Martinez, J., M. M. Bell, J. L. Vigh, and R. F. Rogers, 2017: Examining tropical cyclone structure and intensification with the FLIGHT+ dataset from 1999 to 2012. *Mon. Wea. Rev.*, **145**, 4401–4421, https://doi.org/10.1175/MWR-D-17-0011.1.

Merrill, R. T., 1984: A comparison of large and small tropical cyclones. *Mon. Wea. Rev.*, **112**, 1408–1418, https://doi.org/10.1175/1520-0493(1984)112<1408:ACOLAS>2.0.CO;2.

Montgomery, M. T., and R. J. Kallenbach, 1997: A theory for vortex Rossby- waves and its application to spiral bands and intensity changes in hurricanes. *Quart. J. Roy. Meteor. Soc.*, **123**, 435–465, https://doi.org/10.1002/qj.49712353810.

Montgomery, M. T., M. M. Bell, S. D. Aberson, and M. L. Black, 2006: Hurricane Isabel (2003): New insights into the physics of intense storms. Part I: Mean vortex structure and maximum intensity estimates. *Bull. Amer. Meteor. Soc.*, **87**, 1335–1347, https://doi.org/10.1175/BAMS-87-10-1335.

Powell, M. D., 1982: The transition of the Hurricane Frederic boundary-layer wind field from the open Gulf of Mexico to landfall. *Mon. Wea. Rev.*, **110**, 1912–1932, https://doi.org/10.1175/1520-0493(1982)110<1912:TTOTHF>2.0.CO;2.

Powell, M. D., and T. A. Reinhold, 2007: Tropical cyclone destructive potential by integrated kinetic energy. *Bull. Amer. Meteor. Soc.*, **88**, 513–526, https://doi.org/10.1175/BAMS-88-4-513.

Powell, M. D., E. W. Uhlhorn, and J. D. Kepert, 2009: Estimating maximum surface winds from hurricane reconnaissance measurements. *Wea. Forecasting*, **24**, 868–883, https://doi.org/10.1175/2008WAF2007087.1.

Rozoff, C. M., W. H. Schubert, B. D. McNoldy, and J. P. Kossin, 2006: Rapid filamentation zones in intense tropical cyclones. *J. Atmos. Sci.*, **63**, 325–340, https://doi.org/10.1175/JAS3595.1.

Schneider, R., and G. M. Barnes, 2005: Low - level kinematic, thermodynamic, and reflectivity fields associated with Hurricane Bonnie (1998) at landfall. *Mon. Wea Rev.*, **133**, 3243–3259, https://doi.org/10.1175/MWR3027.1.

Schubert, W. H., M. T. Montgomery, R. K. Taft, T. A. Guinn, S. R. Fulton, J. P. Kossin, and J. P. Edwards, 1999: Polygonal eyewalls, asymmetric eye contraction, and potential vorticity mixing in Hurricanes. *J. Atmos. Sci.*, **56**, 1197–1223, https://doi.org/10.1175/1520-0469(1999)056<1197:PEAECA>2.0.CO;2.

Schubert, W. H., C. M. Rozoff, J. L. Vigh, B. D. McNoldy, and J. P. Kossin, 2007: On the distribution of subsidence in the hurricane eye. *Quart. J. Roy. Meteor. Soc.*, **133**, 595–605, https://doi.org/10.1002/qj.49.

Shapiro, L. J., and M. T. Montgomery, 1993: A three-dimensional balance theory for rapidly rotating vortices. *J. Atmos. Sci.*, **50**, 3322–3335, https://doi.org/10.1175/1520-0469(1993)050<3322:ATDBTF>2.0.CO;2.

Shea, D. J., and W. M. Gray, 1973: The hurricane's inner core region. I. Symmetric and asymmetric structure. *J. Atmos. Sci.*, **30**, 1544–1564, https://doi.org/10.1175/1520-0469(1973)030<1544:THICRI>2.0.CO;2.

Simpson, R. H., 1952: Exploring eye of Typhoon "Marge," 1951. *Bull. Amer. Meteor. Soc.*, **33**, 286–298, https://doi.org/10.1175/1520-0477-33.7.286.

Simpson, R. H., 1955: On the structure of tropical cyclones as studied by aircraft reconnaissance. *Proc. Unesco Symposium on Typhoons*, Tokyo, The Japanese National Committee for UNESCO, 129–150.

Sitkowski, M., and G. M. Barnes, 2009: Low-level thermodynamic, kinematic, and reflectivity fields of Hurricane Guillermo (1997) during rapid intensification. *Mon. Wea. Rev.*, **137**, 645–663, https://doi.org/10.1175/2008MWR2531.1.

Song, J. J., Y. H. Duan, and P. J. Klotzbach, 2020: Revisiting the relationship between tropical cyclone size and intensity over the western North Pacific. *Geophys. Res. Lett.*, **47**, e2020GL088217, https://doi.org/10.1029/2020GL088217.

Vigh, J. L., and Coauthors, 2018: FLIGHT+: The extended flight level dataset for tropical cyclones (Version 1.3). Tropical Cyclone Data Project, National Center for Atmospheric Research, Research Applications Laboratory, Boulder, Colorado.

Wang, Y. Q., 2002a: Vortex Rossby waves in a numerically simulated tropical cyclone. Part I: Overall structure, potential vorticity, and kinetic energy budgets. *J. Atmos. Sci.*, **59**, 1213–1238, https://doi.org/10.1175/1520-0469(2002)059<1213:VRWIAN>2.0.CO;2.

Wang, Y. Q., 2002b: Vortex Rossby waves in a numerically simulated tropical cyclone. Part II: The role in tropical cyclone structure and intensity changes. *J. Atmos. Sci.*, **59**, 1239–1262, https://doi.org/10.1175/1520-0469(2002)059<1239:VRWIAN>2.0.CO;2.

Wang, Y. Q., 2008: Rapid filamentation zone in a numerically simulated tropical cyclone. *J. Atmos. Sci.*, **65**, 1158–1181, https://doi.org/10.1175/2007JAS2426.1.

Willoughby, H. E., 1998: Tropical cyclone eye thermodynamics. *Mon. Wea. Rev.*, **126**, 3053–3067, https://doi.org/10.1175/1520-0493(1998)126<3053:TCET>2.0.CO;2.

Willoughby, H. E., and M. B. Chelmow, 1982: Objective determination of hurricane tracks from aircraft observations. *Mon. Wea. Rev.*, **110**, 1298–1305, https://doi.org/10.1175/1520-0493(1982)110<1298:ODOHTF>2.0.CO;2.

Wu, L. G., W. Tian, Q. Y. Liu, J. Cao, and J. A. Knaff, 2015: Implications of the observed relationship between tropical cyclone size and intensity over the western North Pacific. *J. Climate*, **28**, 9501–9506, https://doi.org/10.1175/JCLI-D-15-0628.1.

Zipser, E. J., R. J. Meitin, and M. A. LeMone, 1981: Mesoscale motion fields associated with a slowly moving gate convective band. *J. Atmos. Sci.*, **38**, 1725–1750, https://doi.org/10.1175/1520-0469(1981)038<1725:MMFAWA>2.0.CO;2.